

The Composition and Evolution of Lithospheric Mantle: a Re-evaluation and its Tectonic Implications

W. L. GRIFFIN^{1*}, SUZANNE Y. O'REILLY¹, J. C. AFONSO^{1,2} AND G. C. BEGG^{1,3}

¹ARC NATIONAL KEY CENTRE FOR GEOCHEMICAL EVOLUTION AND METALLOGENY OF CONTINENTS, DEPARTMENT OF EARTH AND PLANETARY SCIENCES, MACQUARIE UNIVERSITY, N. S.W. 2109, AUSTRALIA

²GDL, INSTITUTE OF EARTH SCIENCES 'J. ALMERA', C.S.I.C., LLUÍS SOLÉ I SABARÍS S/N, 08028, BARCELONA, SPAIN

³MINERALS TARGETING INTERNATIONAL, WEST PERTH, W.A. 6005, AUSTRALIA

RECEIVED JANUARY 27, 2008; ACCEPTED JUNE 12, 2008

The composition of the subcontinental lithospheric mantle (SCLM) is broadly related to the tectonothermal age of the overlying crust, suggesting a secular change in SCLM-forming processes. Most estimated compositions of Archean SCLM, based on well-studied suites of xenoliths and xenocrysts, are depleted garnet lherzolites with high orthopyroxene/olivine. However, these compositions make it difficult to account for the high shear-wave velocities measured in the cores of large cratons, and predict deeper geoid anomalies and higher elevations than are observed in most cratons. Global and regional seismic tomography indicates that most cratonic xenolith suites represent material from the lower-velocity margins of lithospheric blocks. This implies that previous compositional estimates are strongly biased toward metasomatized material. We suggest that most Archean SCLM originally consisted of highly depleted dunites/harzburgites, similar to the Archean orogenic massifs of western Norway. Incorporation of such rocks in the cold upper parts of the cratonic SCLM satisfies the seismic and gravity data, suggesting that large volumes of these rocks are preserved in the cores of cratons, but are poorly sampled by volcanic rocks. The roots of most Proterozoic shields probably consist of refertilized Archean SCLM; the juvenile SCLM beneath Proterozoic and Phanerozoic mobile belts reflects only moderate depletion of Primitive Mantle compositions. Rather than a gradual evolution in SCLM-forming processes, we suggest a sharp dichotomy between Archean and younger tectonic regimes. The differences in buoyancy and viscosity between these two types of SCLM have played a major role in the construction, preservation and recycling of continental crust. If originally Archean

SCLM is more widespread than currently recognized, models of crustal growth rates and recycling may need to be revised.

KEY WORDS: subcontinental lithospheric mantle; mantle evolution; seismic tomography; mantle metasomatism; Archean lithosphere

INTRODUCTION

Earth's continental crust is underlain by the subcontinental lithospheric mantle (SCLM), which ranges in thickness from a few tens of kilometres beneath rift zones to >250 km beneath some Archean cratons. The SCLM consists mainly of ultramafic rocks, ranging from lherzolites (olivine + orthopyroxene + clinopyroxene ± garnet ± spinel) to dunites (olivine) and harzburgites (olivine + orthopyroxene). This compositional range is usually interpreted in terms of the progressive removal of basaltic components during partial melting events. Studies of xenoliths in volcanic rocks and exposed massifs in mobile belts have shown that the mean composition of the SCLM is broadly related to the age of the overlying crust (Griffin *et al.*, 1998, 1999a). Ancient cratons generally are underlain by highly depleted SCLM, whereas most SCLM beneath Phanerozoic mobile belts is only mildly depleted relative to the underlying asthenosphere. Such compositional variations are significant for the tectonic behaviour of the

*Corresponding author. Telephone: +61 2 9850 8954. Fax: +61 2 9850 8943. E-mail: wgriffin@els.mq.edu.au

continental crust, because they affect the buoyancy and rigidity of the lithosphere (Lenardic & Moresi, 1999), and lateral differences in composition and physical properties affect the geodynamic behaviour of the mantle. Understanding the origins of the secular evolution in SCLM composition is important, because different models have different implications for the overall evolution of Earth and for the genetic and tectonic relationships between crust and mantle.

Here we present a re-evaluation of the composition of the Archean SCLM, based on data from mantle petrology, seismic tomography and integrated lithospheric modelling, and propose a new interpretation of the causes of the observed secular evolution in SCLM composition. The conclusions have implications for the formation and destruction of continents, and for estimates of crustal growth rates through time.

SECULAR EVOLUTION IN SCLM COMPOSITION

In the following discussion, volumes of SCLM are classified in terms of the tectonothermal age of the overlying crust, defined as the age of the last major thermal event (Janse, 1994; Griffin *et al.*, 1999a). Archons are areas where the crust has been unaffected since ≥ 2.5 Ga; Protons experienced tectonism at 2.5–1.0 Ga; Tectons have been formed or modified at < 1 Ga.

Estimates of SCLM composition can be derived from peridotite massifs or from xenoliths and xenocrysts in volcanic rocks; each has advantages and drawbacks. Peridotite massifs allow recognition of relationships between different rock types, but such massifs typically are derived from relatively shallow SCLM, and have been deformed and metamorphosed during their tectonic emplacement in the crust. Most examples are found in young mobile belts, and provide little insight into the composition of cratonic SCLM. Exceptions are found in some ultrahigh-pressure metamorphic belts, such as western Norway (Brueckner & Medaris, 1998, 2000), the Qinling–Dabie–Sulu belt of China and the North Qaidam belt of Tibet (e.g. Ye *et al.*, 2000; Song *et al.*, 2004), where fragments of deeper cratonic SCLM have become embedded in subducting continental crust and were exhumed together with that crust when subduction ceased.

Xenolith suites from kimberlites, basalts and other volcanic rocks provide samples from larger vertical sections of the SCLM, but relationships between rock types are seldom obvious. The mantle sample may be biased in terms of the rock types that survived ascent to the surface, as well as in the types of mantle domains sampled by different magma types. Further bias is introduced during sample collection and the choice of samples for analysis; petrologists have favoured garnet-bearing rocks for which

P – T estimates could be made. Compositional estimates derived from averages of the analysed material therefore may be distorted. In cratonic areas, comprehensive and well-studied xenolith suites are derived from a small number of kimberlites, many of them mined for diamonds.

A larger sample, with wider spatial distribution, is provided by xenocrysts of peridotitic wall rocks, extracted from kimberlites and other volcanic rocks. Garnet xenocrysts, in particular, are a rich source of information; the major- and trace-element composition of a peridotitic garnet xenocryst allows an estimate of the temperature, depth and major-element composition of its original host rock, and the Mg-number of the coexisting olivine and orthopyroxene (Griffin *et al.*, 1998, 1999a). The analysis of large numbers of garnets provides an estimate of the mean composition of the SCLM sampled by a given volcanic rock (O'Reilly & Griffin, 2006). Table 1 shows that compositional estimates derived from garnet xenocrysts (Gnt-SCLM, Table 1) are similar to the average composition of xenoliths from the same locality, and the xenocryst data provide information from a much wider range of localities. However, these estimates apply only to the garnet-bearing portion of the SCLM, and thus may give a biased picture of SCLM composition, especially in cratonic areas.

Table 2 compiles estimates of SCLM composition from Archon, Protons and Tectons, based on both garnet xenocrysts and the averages of well-studied xenolith suites. Two estimates for the composition of Primitive Mantle are provided for comparison. Figure 1 summarizes estimates of SCLM composition (Tables 1 and 2) in terms of Ca and Al, two elements that are removed from the mantle residue during the extraction of mafic to ultramafic melts.

'Typical' Archon SCLM, as estimated from garnet xenocrysts and xenolith suites (Table 1; Arc.1, Arc.2, Arc.3) is highly depleted, with CaO and Al₂O₃ in the range of 0.6–1% and 1–1.5%, respectively. In contrast, most Tecton SCLM is only moderately depleted compared with the Primitive Upper Mantle (PUM). Tecton garnet peridotite xenoliths, and Gnt-SCLM estimates, have mean CaO and Al₂O₃ contents of 3.1–3.2% and 3.5–3.9% (vs 3.6% and 4.5% for PUM). Spinel peridotite xenolith suites from Tecton areas are typically somewhat more depleted (mean CaO and Al₂O₃ \approx 2.5% (Table 2), but Re–Os analyses suggest that many of these xenoliths represent relict Proterozoic mantle preserved at shallow depths (Handler *et al.*, 1997; Alard *et al.*, 2002; Xu *et al.*, 2008). Estimates for the mean composition of Proton SCLM spread across the spectrum between these two extremes (Table 1, Fig. 1) with mean CaO and Al₂O₃ contents \approx 2% (Table 2). The secular evolution in composition shown by Fig. 1 has been interpreted (Griffin *et al.*, 1998, 1999a) as reflecting a similar evolution in the processes that produce the SCLM.

The estimate of mean Archon SCLM composition given in Table 1 (Gnt-SCLM, Arc.1) is strongly depleted relative

Table 1: Comparison of Gnt-SCLM and xenolith averages for selected localities

	Kaapvaal <90 Ma South Africa	Kaapvaal	Kaapvaal <90 Ma	Kaapvaal	Daldyn Field Yakutia	Daldyn	Daldyn	Daldyn
	Calc. gnt lherzolite	Median lherzolite	Calc. gnt harzburgite	Median harzburgite	Calc. gnt lherzolite	Median lherzolite	Calc. gnt harzburgite	Median harzburgite
No. samples:	(gnt-SCLM) 335	xenolith 79	(gnt-SCLM) 64	xenolith 24	(gnt-SCLM) 390	xenolith 18	(gnt-SCLM) 180	xenolith 3
SiO ₂	46.0	46.6	45.7	45.9	45.8	44.3	45.4	42.2
TiO ₂	0.07	0.06	0.04	0.05	0.05	0.04	0.02	0.09
Al ₂ O ₃	1.7	1.4	0.9	1.2	1.2	1.0	0.4	0.6
Cr ₂ O ₃	0.40	0.35	0.26	0.27	0.31	0.37	0.18	0.37
FeO	6.8	6.6	6.3	6.4	6.5	7.6	6.1	7.4
MnO	0.12	0.11	0.11	0.09	0.11	0.13	0.11	0.10
MgO	43.5	43.5	45.8	45.2	44.9	45.2	47.2	47.8
CaO	1.0	1.0	0.5	0.5	0.7	1.0	0.2	1.0
Na ₂ O	0.12	0.10	0.06	0.09	0.08	0.07	0.03	0.07
NiO	0.27	0.28	0.30	0.27	0.29	0.29	0.32	0.31
	S. Australia kimberlites	Mt. Gambier S. Australia	Obnazhennaya (N. Siberia)	Obnazhennaya	E. China	E. China	Vitim (Baikhal Rift)	Vitim
	Calc. gnt lherzolite	Median lherzolite	Calc. gnt lherzolite	Median lherzolite	Calc. gnt lherzolite	Median lherzolite	Calc. gnt lherzolite	Median lherzolite
No. samples:	(gnt-SCLM) 335	xenolith 79	(gnt-SCLM) 64	xenolith 24	(gnt-SCLM) 390	xenolith 18	(gnt-SCLM) 180	xenolith 3
SiO ₂	44.4	44.2	44.9	42.6	44.5	45.5	44.5	44.5
TiO ₂	0.07	0.04	0.09	0.00	0.15	0.16	0.15	0.16
Al ₂ O ₃	1.9	1.9	2.4	1.8	3.8	3.8	3.7	4.0
Cr ₂ O ₃	0.41	0.44	0.42	0.44	0.40	0.44	0.40	0.37
FeO	7.8	7.6	7.9	8.4	8.0	8.2	8.0	8.0
MnO	0.13	0.13	0.13	0.13	0.13	0.14	0.13	n.a.
MgO	43.2	43.5	41.7	44.7	39.1	38.1	39.3	39.3
CaO	1.6	1.6	2.1	1.4	3.4	3.3	3.3	3.2
Na ₂ O	0.13	0.05	0.17	0.06	0.27	0.23	0.26	0.32
NiO	0.30	0.29	0.28	0.26	0.25	0.25	0.25	0.25

Calc., calculated; n.a., not analysed.

to the PUM, with a mean Mg-number of 92.7. The low FeO (6.4 wt %) appears to be characteristic of many Archon xenolith suites, and distinguishes these rocks from low Ca–Al peridotites of younger tectonic settings, including Proton and Tecton xenolith suites (Table 2) as well as ophiolites, abyssal peridotites and island-arc mantle, all of which have mean FeO \approx 8% regardless of their degree of depletion (Fig. 2; Griffin *et al.*, 1999a).

In Table 2, calculated modal compositions, density and seismic velocities (V_p , V_s) are given for a series of estimated SCLM compositions of different tectonothermal age; average compositions are drawn from Griffin *et al.* (1999a) and

this work (see discussion below). Two different thermodynamic databases and solution models appropriate to mantle conditions have been used for the calculation of physical properties (Afonso *et al.*, 2008; see the Appendix for details). The modal compositions have been calculated self-consistently by free energy minimization (Connolly, 2005) within the system CFMAS (CaO–FeO–MgO–Al₂O₃–SiO₂). Differences in aggregate density as calculated by these two schemes at relevant T – P – X conditions are insignificant. On the other hand, discrepancies in absolute seismic velocities and modal proportions can become significant for some compositions, although the general

Table 2: Estimates of SCLM composition

	Archons									Models	
	Arc_1	Arc_2	Arc_3	Arc_4	Arc_5	Arc_6	Arc_7	Arc_8	Arc_9	Pm_1	Pm_2
	Av. Archon	Av. Low-T	Av. Low-T	Av. High-T	Av. dunite/harz	Av. lherzolite	Av. dunite/harz	Dunite/Harz	'Primitive'	Prim. Mantle	Prim. Mantle
	Gnt SCLM	xenoliths	xenoliths	lherzolite	Almklovdalen	Almklovdalen	E. Greenland	Tanzania	Archon SCLM	McD. & Sun	Jagoutz <i>et al.</i>
		Kaapvaal	Slave	Kaapvaal	Norway	Norway					
		Craton	Craton	Craton							
SiO ₂	45.7	46.5	42.9	44.3	42.8	43.81	43.0	41.7	42.9	45.0	45.2
TiO ₂	0.04	0.05	0.00	0.17	0.01	0.03	0.00	0.02	0.01	0.20	0.22
Al ₂ O ₃	0.99	1.40	1.10	1.74	0.14	2.2	0.47	0.17	0.30	4.5	4.0
Cr ₂ O ₃	0.28	0.34	0.50	0.30	0.32	0.41	0.43	0.26	0.40	0.38	0.46
FeO	6.4	6.6	7.2	8.1	6.5	7.3	6.5	6.7	6.5	8.1	7.8
MnO	0.11	0.10	0.10	0.12	0.11	0.12	0.19	0.08	0.15	0.14	0.13
MgO	45.5	43.8	47.2	43.3	49.2	43.8	49.0	50.4	49.2	37.8	38.3
CaO	0.59	0.88	0.60	1.27	0.09	1.66	0.12	0.32	0.10	3.6	3.5
Na ₂ O	0.07	0.10	0.12	0.12	0.16	0.27	0.03	0.03	0.10	0.36	0.33
NiO	0.30	0.29	0.31	0.26	0.34	0.31	0.34	0.38	0.34	0.25	0.27
<i>Atomic ratios</i>											
Mg-no.	92.7	92.2	92.1	90.5	93.1	91.5	93.1	93.1	93.1	89.3	89.7
Cr/(Cr + Al)	0.16	0.14	0.10	0.10	0.35	0.04	0.17	0.46	0.23	0.05	0.07
CALCULATED PARAMETERS											
HP database											
<i>100 km, 800°C</i>											
ol/opx/	68.7/26.6/	61.9/31.1/	83.8/10.9/	70.6/19.8/	88.2/11.3/	72.8/14.4/	86.8/11.6/	95.7/2.6/	87.8/11.2/	55.1/17.9/	55.5/19.4/
cpx/gnt	1.5/3.2	2.3/4.7	1.3/3.9	3.5/6.1	0.4/0.1	4.6/8.1	0.0/1.61	1.0/0.7	0.2/0.9	10.0/17	10.9/15
Density (kg/m ³)	3316	3325	3328	3351	3305	3347	3310	3308	3307	3394	3383
V _p (km/s)	8.19	8.16	8.25	8.20	8.25	8.24	8.28	8.30	8.25	8.24	8.23
V _s (km/s)	4.70	4.69	4.71	4.68	4.72	4.70	4.72	4.72	4.72	4.69	4.68
<i>200 km, 1300°C</i>											
ol/opx/	68.8/26.4/	62.1/30.9/	83.9/10.9/	70.7/19.7/	88.3/11.1/	72.9/14.5/	86.9/11.4/	95.8/2.6/	87.8/10.7/	55.2/18.2/	55.6/19.6/
cpx/gnt(spin)	1.3/3.4	2.1/4.9	1.2/4.0	3.3/6.3	0.3/0.2	4.3/8.2	0.0/1.7	1.0/0.7	0.3/1.2	9.4/17.2	9.6/15.2
Density (kg/m ³)	3348	3358	3356	3381	3332	3376	3337	3334	3335	3424	3414
V _p (km/s)	8.21	8.19	8.27	8.21	8.27	8.26	8.28	8.31	8.31	8.26	8.25
V _s (km/s)	4.64	4.63	4.65	4.62	4.65	4.64	4.66	4.66	4.65	4.64	4.63

(continued)

Table 2: *Continued*

Archons									Models		
Arc_1	Arc_2	Arc_3	Arc_4	Arc_5	Arc_6	Arc_7	Arc_8	Arc_9	Pm_1	Pm_2	
Av. Archon	Av. Low- <i>T</i>	Av. Low- <i>T</i>	Av. High- <i>T</i>	Av. dunite/harz	Av. lherzolite	Av. dunite/harz	Dunite/Harz	'Primitive'	Prim. Mantle	Prim. Mantle	
Gnt SCLM	xenoliths Kaaapvaal Craton	xenoliths Slave Craton	lherzolite Kaaapvaal Craton	Almklovdalen Norway	Almklovdalen Norway	E. Greenland	Tanzania	Archon SCLM	McD. & Sun	Jagoutz <i>et al.</i>	
STX database											
<i>100 km, 800°C</i>											
ol/opx/	68.5/25.6/	61.8/29.8/	83.7/9.9/	70.4/18.1/	88.1/11.1/	72.7/12.4/	86.7/11.2/	95.7/2.4/	87.7/10.9/	55.0/13.5/	55.4/15.5/
cpx/gnt(spin)	2.3/3.6	3.4/5.1	2.3/4.1	5.0/6.4	0.4/0.3	6.6/8.3	0.3/1.8	1.2/0.7	0.4/1.1	14.1/17.3	13.8/15.4
Density (kg/m ³)	3316	3324	3329	3351	3306	3348	3310	3310	3308	3394	3383
<i>V_p</i> (km/s)	8.23	8.21	8.29	8.23	8.29	8.28	8.30	8.33	8.30	8.26	8.25
<i>V_s</i> (km/s)	4.71	4.70	4.73	4.69	4.74	4.71	4.74	4.75	4.74	4.67	4.67
<i>200 km, 1300°C</i>											
ol/opx/	68.7/24.8/	61.9/28.6/	83.8/9.2/	70.6/16.9/	88.2/11.0/	72.9/10.8/	86.8/10.9/	95.7/2.2/	87.8/10.7/	55.2/10.5/	55.6/12.6/
cpx/gnt(spin)	2.3/4.2	3.5/5.9	2.3/4.7	5.2/7.4	0.4/0.4	6.8/9.6	0.3/2.1	1.3/0.9	0.3/1.2	14.5/19.8	14.3/17.6
Density (kg/m ³)	3346	3356	3357	3381	3333	3377	3338	3336	3335	3427	3416
<i>V_p</i> (km/s)	8.27	8.26	8.31	8.26	8.30	8.31	8.32	8.33	8.31	8.32	8.30
<i>V_s</i> (km/s)	4.62	4.61	4.64	4.60	4.64	4.62	4.65	4.65	4.65	4.60	4.60

(continued)

Table 2: Continued

	Protons						Tectons			
	Pr_1	Pr_2	Pr_3	Pr_5	Pr_6	Pr_4	Tc_1	Tc_2	Tc_3	Tc_4
	Av. Proton Gnt SCLM	Av. Proton xenoliths	Av. massif peridotite	Lherz Av. harzburgite	Lherz Av. lherzolite	Proton SCLM (preferred)	Av. Tecton Gnt SCLM	Av. Tecton gnt lherzolite	Av. Tecton spinel peridotite	Av. spinel peridotite (McD. & Sun)
SiO ₂	44.7	43.9	45.2	43.9	45.4	44.6	44.5	45.0	44.4	44.0
TiO ₂	0.09	0.04	0.09	0.04	0.15	0.07	0.14	0.16	0.09	0.09
Al ₂ O ₃	2.1	1.6	2.0	0.64	3.7	1.9	3.5	3.9	2.6	2.3
Cr ₂ O ₃	0.42	0.40	0.38	0.29	0.40	0.40	0.40	0.41	0.40	0.39
FeO	7.9	7.9	7.9	8.1	8.3	7.9	8.0	8.1	8.2	8.4
MnO	0.13	0.12	0.11	0.13	0.14	0.12	0.13	0.07	0.13	0.14
MgO	42.4	43.9	41.6	46.0	39.9	42.6	39.8	38.7	41.1	41.4
CaO	1.9	1.3	1.9	0.43	3.2	1.7	3.1	3.2	2.5	2.2
Na ₂ O	0.15	0.08	0.13	0.12	0.26	0.12	0.24	0.28	0.18	0.24
NiO	0.29	0.22	0.28	0.32	0.25	0.26	0.26	0.24	0.27	0.26
<i>Atomic ratios</i>										
Mg-no.	90.6	90.8	90.4	91.9	90.6	90.6	89.9	89.5	89.9	89.8
Cr(Cr + Al)	0.12	0.15	0.11	0.33	0.02	0.12	0.07	0.07	0.09	0.10
CALCULATED PARAMETERS										
HP database										
<i>100 km, 800°C</i>										
ol/opx/	67.3/19.6/	73.4/17.2/	63.3/23.8/	78.5/18.5/	59.9/17.5/	67.9/20.3/	62.1/15.9/	57.3/19.1/	65.8/17.1/	67.9/17.0/
cpx/gnt(spin)	5.6/7.6	3.4/5.9	5.7/7.2	1.1/1.9	9.0/13.6	5.0/6.8	8.9/13.1	9.0/8.45	7.5/9.6	6.6/8.5
Density (kg/m ³)	3354	3346	3354	3333	3382	3351	3378	3385	3367	3365
V _p (km/s)	8.20	8.2	8.17	8.18	8.22	8.20	8.23	8.22	8.20	8.20
V _s (km/s)	4.68	4.68	4.67	4.678	4.68	4.68	4.68	4.68	4.67	4.67
<i>200 km, 1300°C</i>										
ol/opx/	67.4/19.6/	73.4/17.2/	63.5/23.8/	78.6/18.4/	60.0/17.7/	68.0/20.3/	62.2/16.1/	57.4/19.3/	65.9/17.2/	68.0/17.1/
cpx/gnt(spin)	5.3/7.8	3.4/5.9	5.4/7.4	1.0/2.1	8.5/13.8	4.7/7.0	8.5/13.3	8.5/14.9	7.1/9.8	6.3/8.7
Density (kg/m ³)	3385	3376	3385	3363	3412	3382	3407	3416	3397	3395
V _p , km/s	8.22	8.22	8.20	8.20	8.24	8.21	8.25	8.24	8.23	8.22
V _s , km/s	4.62	4.62	4.61	4.616	4.63	4.62	4.63	4.63	4.62	4.61

(continued)

Table 2: *Continued*

	Protons						Tectons			
	Pr_1	Pr_2	Pr_3	Pr_5	Pr_6	Pr_4	Tc_1	Tc_2	Tc_3	Tc_4
	Av. Proton Gnt SCLM	Av. Proton xenoliths	Av. massif peridotite	Lherz Av. harzburgite	Lherz Av. lherzolite	Proton SCLM (preferred)	Av. Tecton Gnt SCLM	Av. Tecton gnt lherzolite	Av. Tecton spinel peridotite	Av. spinel peridotite (McD. & Sun)
STX database										
100 km, 800°C										
ol/opx/	67-2/17-5/	73-2/15-7/	63-2/21-8/	78-3/18-0/	60-1/13-6/	67-8/18-5/	62-0/12-5/	57-2/15-3/	65-7/14-5/	67-8/14-8/
cpx/gnt(spin)	7-4/7-9	5-1/6-0	7-5/7-5	1-5/2-2	12-3/14-0	6-6/7-2	12-2/13-4	12-5/15-0	9-8/9-9	8-7/8-8
Density (kg/m ³)	3354	3347	3353	3333	3383	3352	3378	3385	3367	3366
V _p (km/s)	8-23	8-24	8-2	8-224	8-25	8-22	8-25	8-24	8-23	8-22
V _s (km/s)	4-68	4-69	4-67	4-70	4-67	4-68	4-68	4-67	4-67	4-67
200 km, 1300°C										
ol/opx/	67-3/15-9/	73-3/14-5/	63-3/21-8/	78-5/17-5/	60-2/11-0/	67-9/16-9/	62-1/9-9/	57-4/12-5/	65-8/12-5/	67-9/13-0/
cpx/gnt(spin)	7-7/9-1	5-2/6-9	7-8/8-7	1-6/2-5	12-8/16-0	6-9/8-2	12-6/15-4	13-0/17-1	10-3/11-4	9-1/10-1
Density (kg/m ³)	3385	3376	3385	3362	3414	3382	3410	3417	3398	3396
V _p (km/s)	8-27	8-27	8-25	8-25	8-30	8-26	8-30	8-30	8-27	8-26
V _s (km/s)	4-60	4-60	4-59	4-61	4-60	4-60	4-60	4-60	4-59	4-59

References: McD. & Sun, McDonough & Sun (1995); Jagoutz *et al.*, Jagoutz *et al.* (1979).

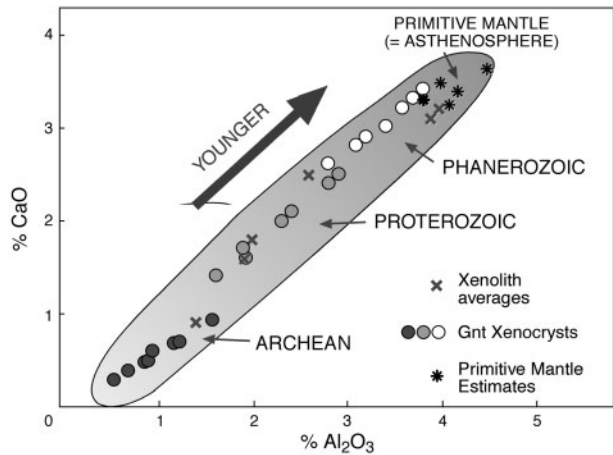


Fig. 1. Secular evolution of SCLM composition, using estimates for single areas based on garnet xenocrysts and xenolith suites (Table 1), and classified in terms of tectonothermal age (after Griffin *et al.*, 1998, 1999a; see this reference for data sources).

response of the system to variations in T – P – X conditions is identical in both schemes. Parallel computations indicate that the inclusion of minor components such as Na_2O and Cr_2O_3 can significantly modify the stability field of the aluminous phases. However, differences in terms of the aggregates' bulk properties are negligible given the uncertainties in end-member thermodynamic parameters. Therefore, we have not included these components in the calculations presented here. Calculated values of modes and physical parameters are given for 100 km depth and 800°C, and 200 km depth and 1300°C, corresponding to two points on a typical cratonic geotherm (40 mW/m²), to allow evaluation of the effects of composition on these parameters.

The 'typical' Archon SCLM derived from garnet xenocryst data (Table 2, Arc.1) has a high opx/olivine ratio compared with PUM and other xenolith suites and massifs. This is because the algorithms used to relate garnet composition to whole-rock composition (Griffin *et al.*, 1999a) are heavily based on the well-studied xenolith suite from the kimberlites of the SW Kaapvaal Craton (Arc.2). However, this high opx/olivine ratio is relatively rare in other xenolith suites (Griffin *et al.*, 1999a) and thus should be regarded with caution. Proton and Tecton SCLM, whether estimated from garnet xenocrysts, xenolith suites or orogenic massifs, show lower opx/olivine, and in general the opx/olivine ratio decreases with increasing degree of depletion (decreasing CaO or Al_2O_3).

Composition is directly reflected in density (Table 1); more depleted rocks have lower density than less depleted ones. The relatively fertile Tecton SCLM is buoyant relative to the underlying asthenosphere when its geotherm is high, but will lose this buoyancy on cooling; it will tend to delaminate, with major tectonic consequences

(e.g. Poudjom Djomani *et al.*, 2001; O'Reilly *et al.*, 2001; Zheng *et al.*, 2006a). In contrast, Archon SCLM is buoyant relative to the asthenosphere, and also is highly refractory. Unmodified Archon SCLM therefore is unlikely to delaminate, or to melt extensively, and would be expected to persist even through major tectonic events. However, it could be modified through time by metasomatic processes, as seen in many xenolith suites, and this refertilization will affect its density and its rheology.

The 'typical' Archon SCLM compositions (Arc.1, 2, 3; Table 2) are consistent with the available xenolith and xenocryst data, and with seismic data from the SW Kaapvaal Craton (James *et al.*, 2001, 2004; O'Reilly & Griffin, 2006; Larson *et al.*, 2006). However, such a composition still presents several problems in terms of geophysical data. Deen *et al.* (2006) pointed out that this composition could only be reconciled with the high shear-wave velocities (V_s) observed in the centres of most cratons by assuming a geotherm significantly cooler (≤ 30 mW/m²) than most xenolith-derived estimates. Afonso *et al.* (2008), using a more sophisticated approach to the calculation of modes, density and seismic velocity, showed that if this composition is assumed to make up the whole SCLM of a typical craton, the predicted geoid anomaly is more negative than the observed values ($\Delta N \approx -100$), and the predicted elevation is significantly higher ($\Delta E \approx 2$ km). It therefore is relevant to ask if the material on which the compositional estimates are based is representative of 'typical' cratonic mantle.

SEISMIC TOMOGRAPHY: MAPPING THE SCLM

Rapid improvements in the quality and resolution of global and regional seismic tomography images are providing new insights into the nature of the SCLM. The global images (e.g. Fig. 3) show that large cratonic areas typically are underlain by high-velocity roots >200 km thick; these are separated by steep gradients from the SCLM beneath mobile belts and rift zones, which has much lower velocities.

Seismic velocity variations in the SCLM commonly are interpreted in terms of temperature differences (variations in the local geotherm). However, this approach is inadequate, because it ignores important links between thickness, composition and geotherm in the SCLM worldwide. The estimated increase in fertility between Archon and Tecton SCLM corresponds to an increase in density (taken at 100 km depth) of 2.0–2.3%, and a decrease in V_s of 1.0–1.4% (Table 2). These compositional variations alone can account for *c.* 20% of the observed range in V_s at depths of 100–175 km beneath the continents (Griffin *et al.*, 1999a). The typical thickness of the depleted SCLM beneath Archons is *c.* 200 km, resulting in low geotherms; the fertile

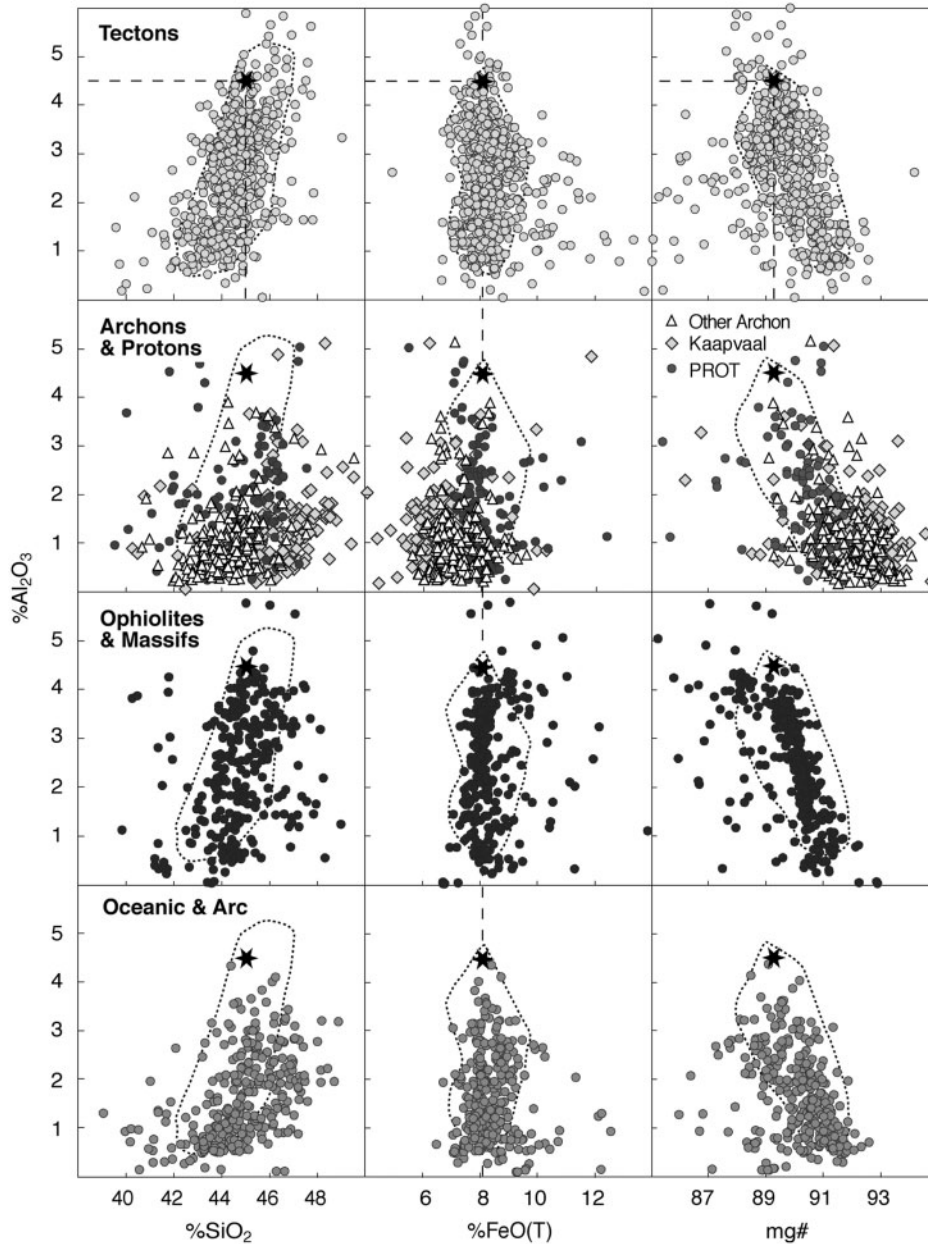


Fig. 2. Covariation of SiO_2 , FeO and mg-number [$100 \text{ Mg}/(\text{Mg} + \text{Fe})$] with Al_2O_3 in xenolith suites, peridotite massifs and oceanic peridotites. Depletion processes in modern oceanic environments produce residues with constant $\text{FeO} = 8 \pm 1 \text{ wt } \%$, and mg-number rises only slowly with increasing depletion. Archean residues have lower FeO and higher mg-number at similar Al_2O_3 contents; the lack of correlation between FeO and SiO_2 shows that the low FeO and high mg-number are not related to high opx/olivine in Archean suites. After Griffin *et al.* (1999a); see this reference for details of data sources. Star shows PUM composition PM₁, Table 2.

SCLM beneath Tectons is typically $<100 \text{ km}$ thick and characterized by high geotherms [see review by O'Reilly & Griffin (2006) and references therein]. Thus greater lithospheric fertility is strongly correlated with higher temperatures and thinner SCLM, all of which lead to lower V_s , whereas greater lithospheric depletion is correlated with low geotherms, thicker SCLM and hence higher V_s . These correlations between composition, thickness and thermal

state reinforce one another to produce rapid lateral changes in density and seismic velocity; they are the key to interpreting the seismic tomography of the SCLM (Deen *et al.*, 2006).

Comparisons of seismic tomography with the thermal and compositional data from xenolith and xenocryst suites provide a basis for using the tomography to map the composition and thermal state of the SCLM. In areas with a relatively high density of mantle-petrology data, such as

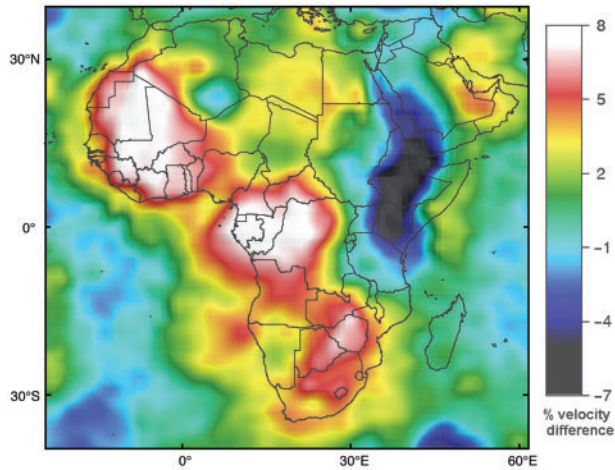


Fig. 3. Seismic tomography (V_s) image of Africa at 100–175 km depth; seismic tomography by S. Grand and BHP Billiton [see Deen *et al.* (2006) for details]. Scale bar shows per cent deviation from PREM model. ‘Hot’ colours (West African, Congo cratons) represent highest V_s (4.79–4.81 km/s), and ‘cold’ colours (e.g. East Africa Rift) lowest V_s (c. 4.1 km/s). Highest V_s in the Kalahari Craton decreases toward the SW, from c. 4.75 km/s beneath parts of Zimbabwe to c. 4.68 km/s in the SW Kaapvaal Craton.

southern Africa, there are broad correlations between seismic velocity, the tectonothermal age of the overlying crust, and the composition and history of the SCLM (Deen *et al.*, 2006; O’Reilly & Griffin, 2006). The highest-velocity SCLM underlies the cores of the Archons (Fig. 3); lower V_s is seen beneath areas where Proterozoic events have affected the crust and mantle (Proton/Archon). These include tectonically reworked areas on the margins of the cratons, or areas affected by major intraplate magmatism (e.g. the Bushveld Complex). Protons, reworked Protons (Tecton/Proton) and Tectons have still lower V_s at the level illustrated in Fig. 3, and these lower velocities can be modelled as a combination of more fertile compositions and somewhat higher geotherms (Deen *et al.*, 2006).

In detail, kimberlites in southern Africa and other cratons tend to be concentrated at the margins of high-velocity SCLM volumes, rather than within them (Griffin *et al.*, 2003; O’Neill *et al.*, 2005; Begg *et al.*, 2008). This is illustrated in Fig. 4, where the locations of kimberlites are plotted on the detailed V_s tomography derived from the Kaapvaal Seismic Project (Fouch *et al.*, 2004). It is especially notable that the kimberlites that have provided some of the best-studied xenolith and xenocryst suites are located on steep velocity gradients along the margins of both high- and low- V_s features. The Kimberley and Prieska areas each lie along a marked low between two highs. The Premier and related pipes lie on the edge of a large low- V_s area marking the centre of the Bushveld intrusion; the Northern Lesotho kimberlites also lie on the edge of a pronounced low- V_s feature. The Jwaneng and Orapa kimberlite fields lie well off the high- V_s areas.

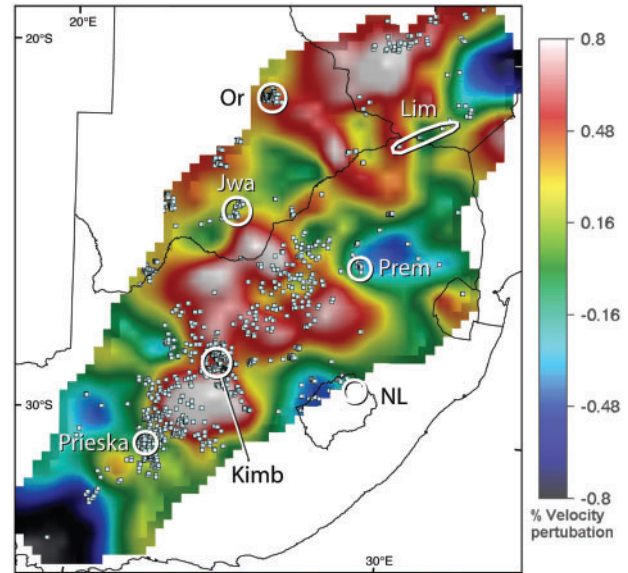


Fig. 4. Detailed V_s tomography at 200 km depth across the SW part of the Kalahari craton of southern Africa (Fouch *et al.*, 2004), with locations of kimberlites (Faure, 2006). Circles and oval mark locations of well-studied xenolith and xenocryst suites. Lim, Limpopo Belt; Prem, Premier (Cullinan) Mine; NL, northern Lesotho; Kimb, Kimberley area; Or, Orapa area; Jwa, Jwaneng area; Prieska area lies across the craton margin. These suites clearly do not sample the highest-velocity parts of the SCLM root.

V_s calculated from mantle samples can reproduce the observed average seismic velocities beneath the sampling localities (James *et al.*, 2004; Larson *et al.*, 2006; O’Reilly & Griffin, 2006), suggesting that the xenoliths may give a representative sample of the SCLM beneath the kimberlite pipes. However, Fig. 4 shows that the xenolith and xenocryst suites on which most estimates of Archon SCLM composition are based do not sample the highest- V_s parts of this cratonic root. The global seismic tomography images (Fig. 3) show that such high- V_s material dominates the cratonic SCLM, whereas the kimberlites have sampled lower- V_s SCLM around the edges of the highest- V_s volumes (Fig. 4; Begg *et al.*, 2008). Figure 3 also shows that even the high- V_s parts of the Kaapvaal Craton actually have lower mean V_s than the main part of the Kalahari Craton to the NW, or the cores of the larger Congo and West African cratons. These observations suggest that the best-studied cratonic xenolith and xenocryst suites are seriously biased toward low- V_s SCLM that is not representative of the bulk of the cratonic roots.

REFERTILIZATION OF DEPLETED SCLM: EVIDENCE FROM XENOLITHS/XENOCRYSTS

Most studies of cratonic garnet peridotite suites have implicitly or explicitly regarded the range of garnet and

clinopyroxene contents as reflecting different degrees of melt extraction from a fertile protolith. Cox *et al.* (1987) recognized that in garnet lherzolite xenoliths, garnet and clinopyroxene commonly are spatially related to one another, and suggested that both phases had been exsolved from high- T Al-rich opx. However, these relationships could also reflect metasomatic introduction of garnet and cpx into a depleted harzburgite, effectively refertilizing a depleted residue.

Xenolith and xenocryst data (e.g. Griffin *et al.*, 2003; Hoal, 2004; Simon *et al.*, 2003, 2007; references therein) suggest that the SCLM in Proton/Archon areas has been extensively refertilized by metasomatic processes, with the addition of Fe, Ca and Al to originally depleted protoliths. Several types of process can be recognized through their fingerprints in xenoliths and garnet xenocrysts. Diamonds and their associated subcalcic garnets probably represent metasomatism of depleted harzburgites by reduced asthenosphere-derived fluids (Malkovets *et al.*, 2007). The high opx/olivine seen in many peridotite xenoliths from the SW part of the Kaapvaal Craton, and sporadically in some other suites, appears to reflect the introduction of Si-rich fluids, possibly related to subduction (e.g. Bell *et al.*, 2005). Clinopyroxene, lherzolitic garnet and phlogopite have been introduced through metasomatism by low-volume fluids in the

kimberlite–carbonatite spectrum. In the Kaapvaal Craton, this style of metasomatism is especially pronounced at depths of 90–150 km, accompanied by an overall reduction in Mg-number and calculated V_s (Fig. 5). The well-studied MARID (Mica–Amphibole–Rutile–Ilmenite–Diopside) metasomatism may be a subset of these processes (Grégoire *et al.*, 2002; references therein). The progressive modification of harzburgite to lherzolite through these processes, accompanied by oxidation, has been demonstrated by studies of zoned garnets in xenoliths (Griffin *et al.*, 1999b; McCammon *et al.*, 2001) and by differences between the matrix minerals of diamond-bearing xenoliths and the corresponding phases included in the diamonds (e.g. Stachel *et al.*, 1998; Creighton *et al.*, 2007; references therein).

A distinctive style of metasomatism is represented by the sheared high- T lherzolite xenoliths found in many kimberlites. Temperatures of 1200–1400°C suggest that many of these are derived from near the base of the SCLM. Strongly zoned garnets and modal correlations between garnet and clinopyroxene suggest that metasomatism has introduced relatively large volumes of both phases shortly before the xenoliths were entrained in the kimberlites (Smith & Boyd, 1987; Griffin *et al.*, 1989; Smith *et al.* 1993). This metasomatism, which appears to be related to the

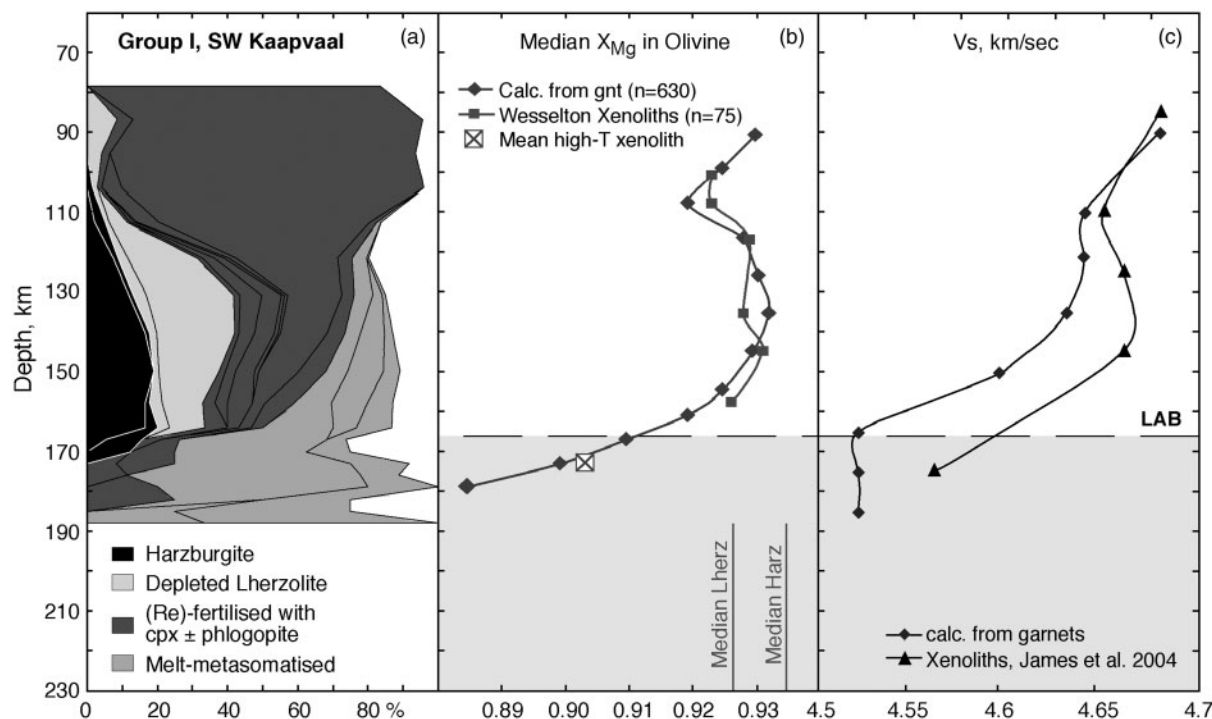


Fig. 5. (a) Chemical tomography section, modified after O'Reilly & Griffin (2006), showing the distribution of garnet-bearing rock types with depth in a composite section of the SCLM based on data from Group 1 kimberlites of the Kimberley area, South Africa (see Fig. 4 for location). (b) Variation with depth of median X_{Mg} in olivine; one curve is calculated from garnet xenocryst data following the method of Gaul *et al.* (2000); the other is based on measured olivine compositions in 75 garnet-bearing xenoliths from the Wesselton mine, Kimberley area. A mean value for olivine in high- T sheared lherzolite xenoliths is shown for comparison. (c) Variation with depth of V_s , as estimated from whole-rock modes and mineral compositions. One curve is calculated from whole-rock compositions estimated from garnet xenocrysts (Griffin *et al.*, 1999a); the other is based on garnet-bearing xenoliths (James *et al.*, 2004).

infiltration of mafic melts (Smith & Boyd, 1987), also leads to a drastic lowering of Mg-number toward the base of the SCLM (Fig. 5b).

The effects of metasomatism on seismic velocity, related to the lowering of Mg-number and the increased modal abundance of garnet, pyroxene and phlogopite, are significant. The overall effect, when combined with increasing temperature, is to produce a strong decrease in V_s with depth within the cratonic SCLM (Fig. 5c). V_p is also affected but shows less of a decrease with depth (James *et al.*, 2004; O'Reilly & Griffin, 2006). We therefore interpret the lowered V_s in the SCLM beneath areas such as Kimberley and Northern Lesotho as reflecting the strong metasomatic refertilization of the SCLM evidenced in xenoliths and xenocrysts from these kimberlite pipes.

Simon *et al.* (2003, 2007) have suggested that garnet and clinopyroxene were introduced into the root of the Kaapvaal craton at around 2.9 Ga, but that most clinopyroxene in low- T granular xenoliths was introduced shortly before kimberlite intrusion (<200 Myr ago). Xenolith and xenocryst data from older kimberlites scattered across the craton (including the Limpopo Belt) show more depleted SCLM, and suggest that the metasomatic modification of the cratonic root has been especially intense over the last 200 Myr (Griffin *et al.*, 2003). However, kimberlites have intruded the Kaapvaal craton in many episodes through time [1700 Ma, 1200 Ma, 500 Ma, 200 Ma, 120–100 Ma, 90–80 Ma, and down to 30 Ma (Batumike *et al.*, 2008)], and other magmatic episodes such as the intrusion of the Bushveld Complex (2050–2060 Ma) and the Karoo volcanism (*c.* 178 Ma) have seriously modified the root (Griffin *et al.*, 2003; Hoal, 2004). It seems probable that the distribution of high- and low- V_s volumes (Figs 3 and 4) reflects the cumulative effects of such magmatic episodes, in which magmas have been focused by pre-existing weaknesses at the boundaries between major lithospheric blocks (Begg *et al.*, 2008).

These metasomatic processes can explain the observed range in V_s without the need to invoke large temperature differences over short lateral distances. This mechanism is consistent with the limited range of palaeogeotherms calculated for xenolith and xenocryst suites from Cretaceous kimberlites across the Kalahari Craton (Griffin *et al.*, 2003; James *et al.*, 2004; Deen *et al.*, 2006). We therefore interpret most of the variation in V_s across this area shown in Fig. 4 as reflecting the metasomatic modification of the cratonic root through time.

REFERTILIZATION OF DEPLETED SCLM: EVIDENCE FROM MASSIF PERIDOTITES

Examples of this refertilization process also are provided by detailed studies of orogenic peridotite massifs.

The Proterozoic continental crust of the Baltic Shield, which was subducted to considerable depths beneath Laurentia during the Caledonian orogeny (Griffin & Brueckner, 1980), contains many large peridotite massifs with well-preserved internal structures (Brueckner & Medaris, 1998, 2000). Preservation of majoritic garnet and diamond indicates that the peridotite bodies were derived from depths up to 200 km (van Roermund *et al.*, 2000, 2001; Brueckner *et al.*, 2002; Spengler *et al.*, 2006; Scambelluri *et al.*, 2008). They are interpreted as fragments of the Laurentian SCLM, entrained in the crust of the Baltic plate during subduction and exhumation. In the Almklovdalen massifs described by Beyer *et al.* (2004, 2006; references therein) small volumes of garnet lherzolite, typically interbanded with eclogite and garnet pyroxenite, occur within large volumes of highly depleted dunite/harzburgite, which are extensively mined for refractory material (Fig. 6; Table 2, Arc.5,6). Whole-rock Re–Os analyses show that the dunite/harzburgite is Archean (*c.* 3 Ga), whereas *in situ* Re–Os analyses show that the garnet lherzolites contain both Archean and Proterozoic sulfides (Beyer *et al.*, 2004), consistent with Proterozoic gnt–cpx Sm–Nd ages on the same rocks (Mearns, 1986; Jamtveit *et al.*, 1991).

The garnet peridotites are interpreted as zones of Proterozoic metasomatic refertilization, related to the intrusion of mafic melts represented by the eclogites and pyroxenites. This refertilization process has added Fe, Ca and Al to the peridotites, crystallizing garnet and clinopyroxene at the expense of olivine and orthopyroxene. It produces chemical trends (Fig. 6) that parallel the 'depletion trend' illustrated in Fig. 1, but run in the opposite direction; these fertilization trends reproduce much of the compositional range seen in garnet lherzolite xenoliths from Archon and Proton settings.

Such refertilization has been recognized previously in numerous studies of European orogenic peridotite massifs and ophiolite complexes, and ascribed to the infiltration of melts, usually in an oceanic setting (e.g. Rampone *et al.*, 1994; Piccardo *et al.*, 2004). In the well-studied Ronda massif, refertilization of a depleted protolith has been linked to heating, partial melting and melt migration on a scale of kilometres, related to asthenospheric upwelling (e.g. Bodinier, 1988; van der Wal & Bodinier, 1996; Garrido & Boudinier, 1999; Lenoir *et al.*, 2001). More recently, Le Roux *et al.* (2007) have demonstrated that the type lherzolite (olivine + opx + cpx + spinel) from the Lherz massif in the Pyrenees (Pr.6, Table 2) was produced by the metasomatic refertilization of a refractory harzburgite (ol + opx ± spinel; Pr.5, Table 2) along a sharply defined front that cross-cuts older structures. Like the Norwegian example, this refertilization process mimics the 'depletion trend' defined by CaO and Al₂O₃ contents (Fig. 6).

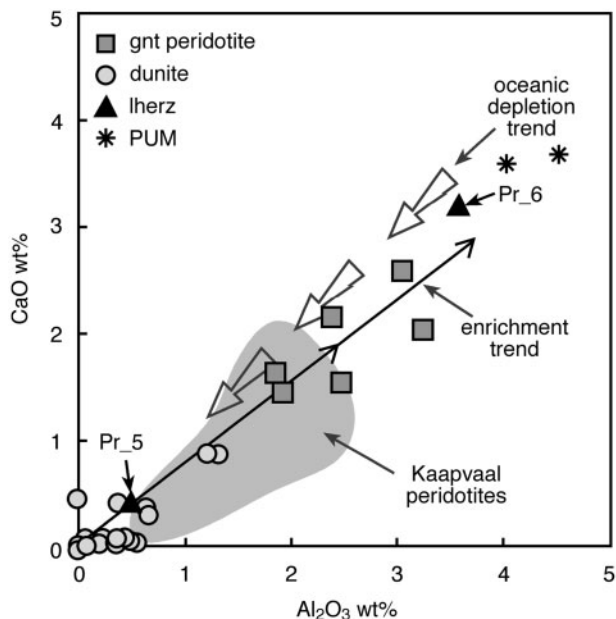


Fig. 6. Compositions of dunites and garnet peridotites from the Archean Almklovtdalen peridotite massif, western Norway (after Beyer *et al.*, 2006). The 'Oceanic Depletion Trend' of Boyd (1989) shows expected compositions of residues after progressive melt extraction from fertile Primitive Mantle compositions. The Norwegian garnet peridotites reflect Proterozoic refertilization of the Archean dunites. This enrichment trend mimics the oceanic trend, but runs in the opposite direction. The difference between the mean compositions of harzburgites (Pr.5; Table 2) and lherzolites (Pr.6; Table 2) from the Lherz massif reflects a similar refertilization process (Le Roux *et al.*, 2007).

The dunite/harzburgite protoliths of the Norwegian peridotites are highly magnesian (Mg-number = 0.93), with high olivine contents. They do not show the high opx/olivine commonly regarded as typical of Archon SCLM (Table 2). Similar highly depleted peridotites have been reported as xenoliths in basalts from East and West Greenland (Bernstein *et al.*, 1998, 2006, 2007). The East Greenland xenolith suite (Bernstein *et al.*, 1998) shows a range of Al contents, with a sharp drop in mean Mg-number and a rise in Cr above 0.6 wt % Al_2O_3 . We interpret this as evidence of refertilization processes similar to those observed in the Norwegian peridotites; the average (Arc.7) shown in Table 2 considers only samples with <0.6% Al_2O_3 . Highly depleted rocks (dunites \pm chromite \pm garnet) make up the upper layer (<140 km depth) of the SCLM beneath the Slave Craton of northern Canada (Pearson *et al.*, 1999; Aulbach *et al.*, 2006). Such depleted compositions (garnet-free harzburgites to dunites) do occur in cratonic xenolith suites (e.g. Bell *et al.*, 2005; Rudnick *et al.*, 1993; Table 2, Arc.8), but are far less well-studied than the more fertile varieties.

The Norwegian garnet peridotites are similar in composition to estimates of Proton SCLM (Table 2, Pr.1, 2, 3) and the high- T sheared peridotites found in many

kimberlites (Table 2, Arc.4). The microstructures and compositions of these sheared xenoliths reflect the infiltration of melts into depleted protoliths, adding Ca, Al, Fe, Na and Ti (Smith & Boyd, 1987; Smith *et al.*, 1993). These comparisons suggest that 'typical Proton' SCLM could be produced by the metasomatic refertilization of originally more depleted Archean protoliths.

DISCUSSION

Secular evolution or abrupt change?

The recognition that metasomatic refertilization can produce the wide range of compositions seen in both Archean garnet peridotites and Proton SCLM has led us to re-examine the crustal history of the areas for which estimates of SCLM composition are available (Fig. 7).

This examination shows that most Proton localities in which the mean SCLM has $\leq 2.5\%$ CaO and Al_2O_3 (Fig. 5; Proton/Archon) contain clear geochronological and isotopic evidence for the Proterozoic reworking of Archean crust. Studies of lower-crustal xenoliths and xenocrystic crustal zircons in volcanic rocks are increasingly providing evidence that the lower crust beneath both Archons and Protons may be significantly older than the bulk of the upper crust (e.g. Zheng *et al.*, 2004, 2007). An example is the Yangtze craton; the exposed upper crust is dominated by Proterozoic rocks with scattered Archean remnants, but the lower crust sampled by lamproite intrusions is dominantly Archean (Zheng *et al.*, 2006b). Several localities for which the mean SCLM composition lies between 3 and 3.5% CaO or Al_2O_3 (e.g. Teiling, North China) represent Phanerozoic reworking of Proterozoic to Archean crust (Fig. 7a; Tecton/Proton), and Phanerozoic thermal events can be inferred to have affected the SCLM as well. Re-Os studies of sulfide populations in mantle xenoliths from some of these areas may reveal still older precursors. Within the Archon suites, the least depleted example is provided by the well-studied xenolith and xenocryst suites from the Group 1 kimberlites of the SW Kaapvaal craton, where the evidence for metasomatic refertilization is most compelling (Griffin *et al.*, 2003; Simon *et al.*, 2003, 2007).

Rather than a secular evolution in the processes that have produced the SCLM, the data appear to favour a dichotomy in process (Fig. 7b). On the one hand, primitive Archon SCLM may be represented by the most depleted examples, such as the Norwegian peridotites. Metasomatic refertilization of these refractory protoliths over time, and especially during episodes of subduction, collision and magmatism, could produce the range of composition seen in Archon SCLM and, eventually, the more fertile Proton SCLM. On the other hand, the moderate depletion of material similar to the Primitive Upper Mantle may have produced juvenile SCLM with 2.5–4% Al_2O_3 , as seen beneath some Proterozoic terrains (e.g. Gao *et al.*, 2002),

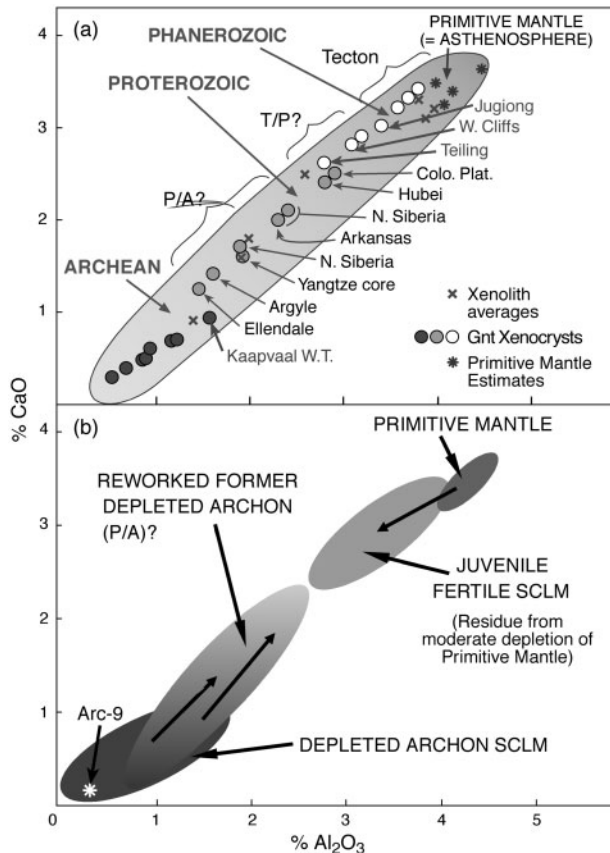


Fig. 7. Secular evolution of the SCLM. (a) More detailed classification of localities shown in Fig. 1, in terms of tectonothermal age and prehistory; P/A represents areas with Archean crust reworked in Proterozoic time; T/P, Proterozoic crust reworked in Phanerozoic time. (b) Reinterpretation of the 'secular evolution' trend; primary Archon SCLM (Arc.9; Table 2) is highly depleted, and its refertilization has produced most 'Proton' (P/A) SCLM. However, some juvenile Protons (mainly Proterozoic mobile belts) are underlain by relatively fertile SCLM, produced by moderate depletion of primitive mantle compositions, as in most Tecton areas.

and most Tectons (Griffin *et al.*, 1999a; Xu *et al.*, 2000; Tables 1 and 2).

Estimated composition of the 'pristine Archon' SCLM

We interpret the seismic tomography data as showing that the upper 100–150 km of the SCLM beneath large cratonic areas (e.g. Africa, Siberia, North America; Deen *et al.*, 2006) is more strongly depleted than the garnet lherzolites that previously have been accepted as representative of the Archean SCLM. Some estimates of Archon SCLM composition derived from garnet xenocryst data are depleted (down to 0.5% Al₂O₃; Fig. 1), but even these estimates can only define the composition of the garnet-bearing portion of the SCLM. If much of the garnet in these rocks is metasomatic, the original SCLM must be even more

depleted. To understand the original nature of the Archon SCLM, and the bulk composition of the major cratonic roots, we must try to extrapolate back to the less metasomatized protoliths.

A better estimate of the composition of the depleted Archean SCLM can be derived by combining data from the Norwegian massifs and the most depleted (least refertilized?) xenoliths from Greenland (Bernstein *et al.*, 1998, 2006, 2007), the Slave Province (Pearson *et al.*, 1999; Aulbach *et al.*, 2006) and Tanzania (Rudnick *et al.*, 1993). Several of these suites show a strong negative correlation between Al and Mg-number below 0.6–1% Al₂O₃ (Fig. 2), which may reflect either progressive depletion or metasomatic refertilization. We therefore have selected samples with <0.6% Al₂O₃ to construct a proposed average composition (Arc.9 in Table 2). It has lower Al, Si and Ca than previous estimates of the Archean SCLM, and higher MgO. We suggest that this composition is representative of the 'pristine' Archean SCLM, and that it extends to considerable depths in the cores of major cratons, where it is poorly sampled by kimberlites and other volcanic rocks. Bernstein *et al.* (2007) have suggested that a similar, though slightly less depleted rock type (Mg-number = 92.8) makes up much of the shallow SCLM worldwide. The oldest known kimberlites, the 1.8 Ga Brockman Creek dykes in the Pilbara Craton of Australia, have sampled extremely depleted roots, consisting largely of magnesian harzburgites (Wyatt *et al.*, 2002; mean Mg-number of olivine = 93.3), and these also may be representative of 'pristine Archon' SCLM.

The proposed dunite/harzburgite composition (Arc.9), like many Archon xenolith suites, is also remarkably low in Fe, and this makes it essentially unique to the Archean SCLM. As noted above, peridotites (ranging from lherzolite through harzburgite to dunite) from modern oceanic environments have nearly uniform Fe (FeO_T ≈ 8 ± 1%; Fig. 2), even at the highest degrees of depletion. Some Archon xenoliths, mainly from the SW Kaapvaal craton, have high opx/olivine ratios, but the low FeO contents are independent of Si content. Low FeO thus is not related to the metasomatic introduction of opx (Bell *et al.*, 2005), but appears to be a fundamental primary property of Archon SCLM.

The proposed 'pristine' Archon SCLM composition, although significantly more depleted than the earlier estimates, has a similar density, but a noticeably higher V_p and V_s (Table 2). The differences in density and seismic velocity reflect the lower opx/olivine of the new estimate. Assuming cratonic geotherms similar to those observed in many kimberlite-borne xenolith suites, this composition will yield the high seismic velocities observed beneath the cratonic cores (Fig. 3; Table 2). Afonso *et al.* (2008) have demonstrated that a cratonic SCLM in which the upper 100–150 km consists of this highly depleted composition,

and the lower part becomes progressively more fertile with depth (see Fig. 5b), produces a geoid anomaly within the observed ranges, a mean elevation of 400–500 m, and a velocity–depth profile that matches that of typical cratonic regions.

Origin of the depleted Archean SCLM

Experimental studies of the progressive melting of pyrolite compositions (e.g. Walter, 1998, 1999; Herzberg, 1999) allow estimates of the depth and degree of melting represented by possible residual compositions. Comparisons with these experimental studies indicate that the ‘pristine Archean’ dunite/harzburgite composition (Arc.9) proposed here represents the residue of >50% melting at pressures around 5 GPa (Fig. 8).

However, this approach can be applied only to melt residues; the effects of metasomatic refertilization will produce spurious results. Thus the average compositions derived from Kaapvaal xenoliths (Arc.2) give very high estimated pressures (>7 GPa), as a result of their high opx/olivine ratios. We regard these high opx contents as a localized phenomenon, related to deep-seated metasomatism.

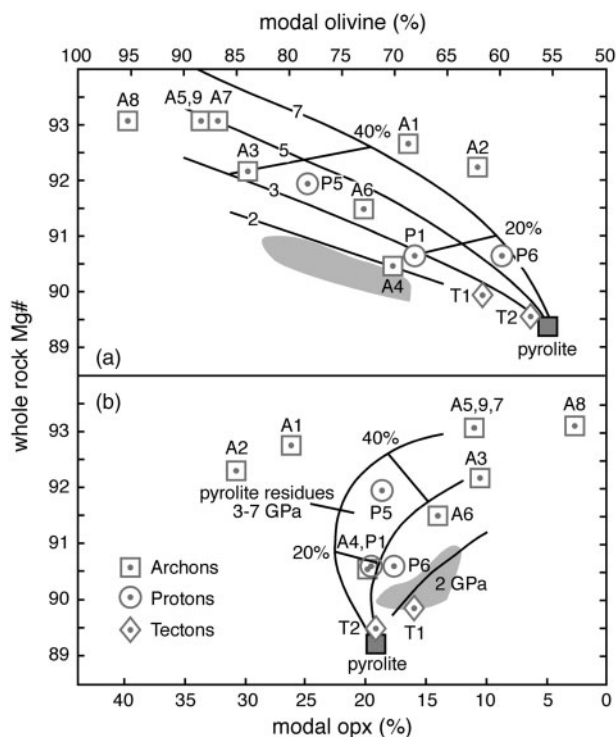


Fig. 8. Comparison of SCLM compositions with residues produced by melting of a fertile peridotite at pressures from 2 to 7 GPa (c. 60–220 km depth); grey field represents abyssal oceanic peridotites (after Walter, 1998). Data from Table 2; A, Archon SCLM estimates; P, Proton SCLM estimates; T, Tecton SCLM estimates. Our preferred estimate of the primary Archon SCLM composition (A9), and the Norwegian and Greenland dunite/harzburgites (A5, A7), would be generated by high-degree melting at pressures ≥ 5 GPa.

As noted above, this high opx/olivine ratio is propagated into the SCLM composition derived from garnet xenocrysts (Arc.1). The harzburgite protoliths of the Lherz massif (Pr.5) yield reasonable pressures of 3–4 GPa at <40% melt extraction, whereas the metasomatic lherzolites give higher P estimates that are inconsistent with their spinel-facies mineralogy. Similarly, the high- T sheared lherzolite xenoliths from Kaapvaal Craton kimberlites (Arc.4) give pressures of 2 GPa, which are inconsistent with P – T estimates derived from mineral equilibria (typically 1200–1400°C, 4–6 GPa). The metasomatic garnet lherzolites within the Norwegian dunite/harzburgite massifs yield pressures of 3–4 GPa, in the lower range of the P – T estimates for the garnet-bearing assemblages based on mineral equilibria (Brueckner & Medaris, 1998). This agreement may reflect the conditions at which metasomatic refertilization of the dunites occurred, or it may be a coincidence; in either case, the estimated pressure cannot reflect a depth of melt depletion.

We suggest the same may be true of the lower P suggested by the composition of Proton SCLM (Pr.1, 2). However, the lower pressures calculated for Tecton garnet and spinel peridotites may reflect an origin through modern plate-tectonic processes, with depletion beneath mid-ocean ridges and island arcs.

Several studies (e.g. Canil, 2004; references therein) have used modelling of major- and trace-element data to argue that cratonic xenoliths retain a signature of melt depletion at shallow depths, and that the cratonic SCLM has been built up by the stacking of oceanic slabs beneath pre-existing continents. However, we suggest that this approach produces misleading results, because the cratonic xenolith sample (as represented in the literature) is dominated by rocks that are not simple residues from partial melting. They are the products of metasomatic refertilization and thus cannot be compared with experimentally produced residues or melting trends.

The data from the orogenic peridotite massifs show that the refertilization processes raise the levels of all commonly accepted measures of fertility or depletion, including the large ion lithophile elements, heavy rare earth elements (including Y and Yb), high field strength elements, and ‘mildly incompatible’ elements such as V, Ga and Cr. For example, in the refertilized Norwegian peridotites, all of these elements show strong positive correlations with whole-rock CaO, FeO and Al₂O₃ contents, whereas Ni and Co contents decrease with increasing CaO and Al₂O₃ (Beyer *et al.*, 2006). These correlations indicate that it is impossible to ‘see through’ such metasomatic refertilization, and to use individual elements, groups of elements or element ratios to derive the conditions under which the protoliths of these rocks were formed. The best guide to formation conditions thus will be found in the most strongly depleted, least refertilized rocks.

The high Cr/Al of the harzburgitic garnets and chromites found as inclusions in diamond and in some diamond-bearing xenoliths is commonly advanced as evidence for the low- P origin of cratonic SCLM, because experimental melting studies have failed to produce such signatures at high P (e.g. Kesson & Ringwood, 1989; Kelemen *et al.*, 1998; Stachel *et al.*, 1998; Canil, 2004; Bernstein *et al.*, 2007). However, this high-Cr-number signature is also readily explained by metasomatic processes. Malkovets *et al.* (2007) have argued that the depth distribution of diamond, subcalcic garnet and chromite as sampled by kimberlites reflects the formation of both diamonds and G10 garnets by a metasomatic redox process that can be expressed schematically as $\text{Opx (Ca, Al) + chromite (Cr, Al, Fe}^{3+}) + \text{CH}_4$ (in asthenosphere-derived fluids) \rightarrow C (diamond or graphite) + $\text{H}_2\text{O} + \text{garnet (high-Cr) + Opx (low-Ca, Al) + chromite (high-Cr-number; Fe}^{2+})$. This reaction is consistent with other models for diamond formation by oxidation of reduced asthenosphere-derived fluids (e.g. Maruoka *et al.*, 2004). Thus high Cr-number in spinel or garnet can be explained as a metasomatic signature produced in the deep lithosphere, and is not evidence for a low- P origin for the protoliths of cratonic SCLM. It should be noted that single depleted peridotite xenoliths from kimberlites and basalts may have Cr_2O_3 ranging from <0.1 to $>2.0\%$, and Cr-number ranging from 0.2 to 1 (Bernstein *et al.*, 1998, 2006; Griffin *et al.*, 1999a), probably reflecting modal sorting of pyroxene, olivine and spinel. The estimated Cr_2O_3 content of the Arc.9 composition therefore is difficult to constrain within a factor of two.

We suggest that the original Archean SCLM is best represented by a strongly depleted dunite/harzburgite composition (Arc.9; Table 2) that formed by high-degree partial melting at pressures ≥ 5 GPa. This high- P melting may have begun in rising plumes or mantle upwellings, producing the low FeO contents characteristic of Archean SCLM (Fig. 2). Bernstein *et al.* (2007) have suggested that this melting continued to the point of exhaustion of orthopyroxene in the residue, whereas our estimated composition would allow the retention of *c.* 10% opx. The positive correlation between Al and Cr in some depleted Archean xenolith suites has been cited as an argument for the exhaustion of both spinel and garnet during the melt extraction (Griffin *et al.*, 1999a), implying that spinel may later have exsolved from high- T opx during cooling. However, a later metasomatic enrichment in both elements cannot be ruled out as the cause of this correlation.

The dichotomy between Archean processes and those that formed the younger SCLM is illustrated by the data from the Lherz massif (Le Roux *et al.*, 2007). Although the primitive harzburgite protolith (Pr.5; Table 2) has Al and Ca contents lower than those of many Archean xenolith suites (see Table 1), it has the FeO content ($8 \pm 1\%$)

characteristic of all estimates of Proton and Tecton SCLM, abyssal peridotites and xenoliths from arc-related mantle, regardless of their degree of depletion. This dichotomy strongly suggests that the processes that produced the low-Fe Archean SCLM have not operated since the end of the Archean.

Continental crust and the SCLM

Thick sections of highly depleted Archon SCLM are buoyant relative to the convecting mantle on typical cratonic geotherms (Poudjom Djomani *et al.*, 2001). Its anhydrous composition will give the Archon SCLM a high degree of rigidity (e.g. Afonso & Ranalli, 2004), and both factors will help it to survive even major tectonic processes. Metasomatism may decrease its buoyancy and viscosity, especially in the deeper lithosphere, but most Proton SCLM compositions will remain buoyant relative to the asthenosphere (Poudjom Djomani *et al.*, 2001; O'Reilly *et al.*, 2001). We therefore suggest that many Proterozoic shields, particularly in areas where an Archean crustal prehistory can be detected in the upper or lower crust, have SCLM roots that were generated in Archean time.

If this interpretation is correct, it suggests that the area (volume) of continental SCLM has remained relatively constant at least since the end of the Archean. This buoyant SCLM would have provided 'life rafts' on which Archean crust could be preserved from recycling. Detailed geochronological and geochemical studies of crustal xenoliths (e.g. Zheng *et al.*, 2004, 2006a, 2007) suggest that this ancient crust has been extensively 'resurfaced' in many areas, and is still preserved at depth. If the high-velocity SCLM beneath large areas of the present continents (e.g. Deen *et al.*, 2006) is in fact relict Archean SCLM, then Archean crust probably is similarly widespread, and thus is more voluminous than commonly recognized. Measurements of crustal growth rates based on surface geology therefore would require revision to allow for a higher rate of crustal growth in the early Archean. This has major implications for mechanisms of crustal growth, recycling and lithosphere evolution (e.g. Armstrong, 1991), and for global geodynamic and geochemical models.

ACKNOWLEDGEMENTS

The ideas presented here have been developed through many discussions with Jon Hronsky, Lev Natapov, Norman Pearson, Craig O'Neill and Olivier Alard. Steve Grand provided an updated version of his global seismic tomography model and helped us to understand many aspects of its use to investigate the lithosphere. The digital version of Fig. 4 was provided by BHP Billiton. We thank J. Connolly for providing the necessary files and subroutines for the energy minimization calculations (<http://www.perplex.ethz.ch/>). The manuscript was improved by

critical reviews from Doug Smith, Stefan Bernstein and David James. The analytical data were obtained using instrumentation funded by ARC LIEF, and DEST Systemic Infrastructure Grants, industry partners and Macquarie University. This work would have been impossible without the enthusiastic help of the staff of the Geochemical Analysis Unit over many years. The research was supported by ARC and Macquarie University grants to S.Y.O'R. and W.L.G., and collaborative research with industry partners. This is contribution 542 from the ARC National Key Centre for Geochemical Evolution and Metallogeny of Continents (www.es.mq.edu.au/GEMOC).

REFERENCES

- Afonso, J. C. & Ranalli, G. (2004). Crustal and mantle strengths in continental lithosphere: is the jelly sandwich model obsolete? *Tectonophysics* **394**, 221–232.
- Afonso, J. C., Fernandez, M., Ranalli, G., Griffin, W. L. & Connolly, J. A. D. (2008). Integrated geophysical–petrological modeling of the lithosphere and sublithospheric upper mantle: methodology and applications. *Geochemistry, Geophysics, Geosystems* **9**, Q05008, doi:10.1029/2007GC001834.
- Alard, O., Griffin, W. L., Pearson, N. J., Lorand, J.-P. & O'Reilly, S. Y. (2002). New insights into the Re–Os systematics of subcontinental lithospheric mantle from *in-situ* analysis of sulfides. *Earth and Planetary Science Letters* **203**, 651–663.
- Armstrong, R. L. (1991). The persistent myth of crustal growth. *Australian Journal of Earth Science* **38**, 613–630.
- Aulbach, S., Griffin, W. L., Pearson, N. J., O'Reilly, S. Y., Kivi, K. & Doyle, B. J. (2006). Mantle formation and evolution, Slave Craton: constraints from HSE abundances and Re–Os systematics of sulfide inclusions in mantle xenocrysts. *Chemical Geology* **208**, 61–88.
- Batumike, J. M., Griffin, W. L., Belousova, E. A., Pearson, N. J., O'Reilly, S. Y. & Shee, S. R. (2008). LAM-ICPMS U–Pb dating of kimberlitic perovskite: Eocene–Oligocene kimberlites from the Kundelungu Plateau, D.R. Congo. *Earth and Planetary Science Letters* **267**, 609–619.
- Bell, D. R., Grégoire, M., Grove, T. L., Chatterjee, N., Carlson, R. W. & Buseck, P. R. (2005). Silica and volatile-element metasomatism of Archean mantle: a xenolith-scale example from the Kaapvaal Craton. *Contributions to Mineralogy and Petrology* **150**, 251–267.
- Bernstein, S., Kelemen, P. B. & Brooks, C. K. (1998). Depleted spinel harzburgite xenoliths in Tertiary dikes from East Greenland: restites from degree melting. *Earth and Planetary Science Letters* **154**, 221–235.
- Bernstein, S., Hanghoi, K., Kelemen, P. B. & Brooks, C. K. (2006). Ultra-depleted shallow cratonic mantle beneath West Greenland: dunitic xenoliths from Ubekendt Eiland. *Contributions to Mineralogy and Petrology* **152**, 335–347.
- Bernstein, S., Kelemen, P. B. & Hanghoi, K. (2007). Consistent olivine Mg# in cratonic mantle reflects Archean mantle melting to the exhaustion of orthopyroxene. *Geology* **35**, 459–462.
- Beyer, E. E., Brueckner, H. K., Griffin, W. L., O'Reilly, S. Y. & Graham, S. (2004). Archean mantle fragments in Proterozoic crust, Western Gneiss Region, Norway. *Geology* **32**, 609–612.
- Beyer, E. E., Griffin, W. L. & O'Reilly, S. Y. (2006). Transformation of Archean lithospheric mantle by refertilisation: evidence from exposed peridotites in the Western Gneiss Region, Norway. *Journal of Petrology* **47**, 1611–1636.
- Bodinier, J.-L. (1988). Geochemistry and petrogenesis of the Lanzo peridotite body, Western Alps. *Tectonophysics* **149**, 67–88.
- Boyd, F. R. (1989). Composition and distinction between oceanic and cratonic lithosphere. *Earth and Planetary Science Letters* **96**, 15–26.
- Brueckner, H. K. & Medaris, L. G. (1998). A tale of two orogens: the contrasting *T–P–t* history and geochemical evolution of mantle in high- and ultrahigh-pressure metamorphic terranes of the Norwegian Caledonides and the Czech Variscides. *Schweizerische Mineralogische und Petrographische Mitteilungen* **78**, 293–307.
- Brueckner, H. K. & Medaris, L. G., Jr (2000). A general model for the intrusion and evolution of 'mantle' peridotites in high-pressure and ultrahigh-pressure metamorphic terranes. *Journal of Metamorphic Geology* **18**, 119–130.
- Brueckner, H. K., Carswell, D. A. & Griffin, W. L. (2002). Paleozoic diamonds within a Precambrian peridotite lens in UHP gneisses of the Norwegian Caledonides. *Earth and Planetary Science Letters* **203**, 805–816.
- Canil, D. (2004). Mildly incompatible elements in peridotites and the origins of mantle lithosphere. *Lithos* **77**, 375–393.
- Connolly, J. A. D. (2005). Computation of phase equilibria by linear programming: a tool for geodynamic modelling and its application to subduction zone decarbonation. *Earth and Planetary Science Letters* **236**, 524–541.
- Cox, K. G., Smith, M. R. & Beswetherick, S. (1987). Textural studies of garnet lherzolites: evidence of exsolution origin from high-temperature harzburgites. In: Nixon, P. H. (ed.) *Mantle Xenoliths*. New York: John Wiley, pp. 537–550.
- Creighton, S., Stachel, T., McLean, H., Muehlenbachs, K., Simonetti, A., Eichenberg, D. & Luth, R. (2007). Diamondiferous peridotitic microxenoliths from the Diavik diamond mine, NT. *Contributions to Mineralogy and Petrology* doi:10.1007/s00410-007-0257-x.
- Deen, T., Griffin, W. L., Begg, G., O'Reilly, S. Y. & Natapov, L. M. (2006). Thermal and compositional structure of the subcontinental lithospheric mantle: Derivation from shear-wave seismic tomography. *Geochemistry, Geophysics, Geosystems* doi:10.1029/2005GC001164.
- Faure, S. (2006). World Kimberlites Database Version 2006–2. Montreal, Que.: Consortium de Recherche en Exploration Minérale CONSOREM, Université du Québec à Montréal. www.consorem.ca.
- Fouch, M. J., James, D. E., VanDecar, J. C., van der Lee, S. & the Kaapvaal Seismic Group (2004). Mantle seismic structure beneath the Kaapvaal and Zimbabwe Cratons. *South African Journal of Geology* **107**, 33–44.
- Fuhrman, M. L. & Lindsley, D. H. (1988). Ternary-feldspar modelling and thermometry. *American Mineralogist* **73**, 201–215.
- Gao, S., Rudnick, R. L., Carlson, R. W., McDonough, W. F. & Liu, Y.-S. (2002). Re–Os evidence for replacement of ancient mantle lithosphere beneath the North China craton. *Earth and Planetary Science Letters* **198**, 307–322.
- Garrido, C. & Bodinier, J.-L. (1999). Diversity of mafic rocks in the Ronda peridotite: evidence for pervasive melt/rock reaction during heating of subcontinental lithosphere by upwelling asthenosphere. *Journal of Petrology* **40**, 729–754.
- Gaul, O. F., Griffin, W. L., O'Reilly, S. Y. & Pearson, N. J. (2000). Mapping olivine composition in the lithospheric mantle. *Earth and Planetary Science Letters* **182**, 223–235.
- Grégoire, M., Bell, D. R. & Le Roux, A. P. (2002). Trace element geochemistry of phlogopite-rich mafic mantle xenoliths: their classification and their relationship to phlogopite-bearing peridotites and kimberlites revisited. *Contributions to Mineralogy and Petrology* **142**, 603–625.
- Griffin, W. L. & Brueckner, H. K. (1980). Caledonian Sm–Nd ages and a crustal origin for Norwegian eclogites. *Nature* **285**, 319–320.

- Griffin, W. L., Smith, D., Boyd, F. R., Cousens, D. R., Ryan, C. G., Sie, S. H. & Suter, G. F. (1989). Trace element zoning in garnets from sheared mantle xenoliths. *Geochimica et Cosmochimica Acta* **53**, 561–567.
- Griffin, W. L., O'Reilly, S. Y., Ryan, C. G., Gaul, O. & Ionov, D. (1998). Secular variation in the composition of subcontinental lithospheric mantle. In: Braun, J., Dooley, J. C., Goleby, B. R., van der Hilst, R. D. & Klootwijk, C. T. (eds) *Structure and Evolution of the Australian Continent. American Geophysical Union, Geodynamics Series* **26**, 1–26.
- Griffin, W. L., O'Reilly, S. Y. & Ryan, C. G. (1999a). The composition and origin of subcontinental lithospheric mantle. In: Fei, Y., Bertka, C. M. & Mysen, B. O. (eds) *Mantle petrology: field observations and high pressure experimentation: a tribute to Francis F. (Joe) Boyd*. The Geochemical Society, pp. 13–45.
- Griffin, W. L., Shee, S. R., Ryan, C. G., Win, T. T. & Wyatt, B. A. (1999b). Harzburgite to lherzolite and back again: Metasomatic processes in ultramafic xenoliths from the Wesselton kimberlite, Kimberley, South Africa. *Contributions to Mineralogy and Petrology* **134**, 232–250.
- Griffin, W. L., O'Reilly, S. Y., Natapov, L. M. & Ryan, C. G. (2003). The evolution of lithospheric mantle beneath the Kalahari Craton and its margins. *Lithos* **71**, 215–242.
- Handler, M. R., Bennett, V. C. & Esat, T. M. (1997). The persistence of off-cratonic lithospheric mantle: Os isotopic systematics of variably metasomatised southeast Australian xenoliths. *Earth and Planetary Science Letters* **151**, 51–75.
- Herzberg, C. (1999). Phase equilibrium constraints on the formation of mantle. In: Fei, Y., Bertka, C. M. & Mysen, B. O. (eds) *Mantle Petrology: Field Observations and High Pressure Experimentation: a Tribute to Francis F. (Joe) Boyd*. Geochemical Society, Special Publication **6**, 241–258.
- Hoal, K. O. (2004). Samples of Proterozoic iron-enriched mantle from the Premier kimberlite. *Lithos* **71**, 259–272.
- Holland, T. & Powell, R. (1996). Thermodynamics of order–disorder in minerals: 2. Symmetric formalism applied to solids solutions. *American Mineralogist* **81**, 1425–1437.
- Holland, T. & Powell, R. (1998). An internally consistent thermodynamic data set for phases of petrological interest. *Journal of Metamorphic Geology* **16**, 309–343.
- Jagoutz, E., Palme, H., Baddenhausen, H., Blum, K., Cendales, M., Dreibus, G., Spettel, B., Lorenz, V. & Wanke, H. (1979). The abundance of major, minor and trace elements in the Earth's mantle as derived from primitive ultramafic nodules. *Proceedings of the 10th Lunar and Planetary Science Conference. Geochimica et Cosmochimica Acta Supplement* 2031–2050.
- James, D. E., Fouch, M. J., VanDecar, J. C., van der Lee, S. & Kaapvaal Seismic Group (2001). Tectospheric structure beneath southern Africa. *Geophysical Research Letters* **28**, 2485–2488.
- James, D. E., Boyd, F. R., Schutt, D., Bell, D. R. & Carlson, R. W. (2004). Xenolith constraints on seismic velocities in the upper mantle beneath southern Africa. *Geochemistry, Geophysics, Geosystems* **5**, doi:10.1029/2003GC000551.
- Jamtveit, B., Carswell, D. A. & Mearns, E. W. (1991). Chronology of the high-pressure metamorphism of Norwegian garnet peridotites/pyroxenites. *Journal of Metamorphic Geology* **9**, 1–15.
- Janse, A. J. A. (1994). Is Clifford's Rule still valid? Affirmative examples from around the world. In: Meyer, H. O. A. & Leonardos, O. (eds) *Diamonds: Characterization, Genesis and Exploration. CPRM Special Publication* **1A/93**, 215–235.
- Kelemen, P. B., Hart, S. R. & Bernstein, S. (1998). Silica enrichment in the continental lithosphere via melt/rock reaction. *Earth and Planetary Science Letters* **164**, 387–406.
- Kesson, S. E. & Ringwood, A. E. (1989). Slab–mantle interactions 2. The formation of diamonds. *Chemical Geology* **78**, 97–118.
- Larson, A. M., Snoke, J. A. & James, D. E. (2006). S-wave velocity structure, mantle xenoliths and the upper mantle beneath the Kaapvaal craton. *Geophysics Journal International* **167**, 171–186.
- Lenardic, A. & Moresi, L. N. (1999). Some thoughts on the stability of cratonic lithosphere: effects of buoyancy and viscosity. *Journal of Geophysical Research* **104**, 12747–12758.
- Lenoir, X., Garrido, C., Bodinier, J.-L., Dautria, J.-M. & Gervilla, F. (2001). The recrystallization front of the Ronda peridotite: evidence for melting and thermal erosion of subcontinental lithospheric mantle beneath the Alboran Basin. *Journal of Petrology* **42**, 141–158.
- Le Roux, V., Bodinier, J.-L., Tommasi, A., Alard, O., Dautria, J.-M., Vauchez, A. & Riches, A. J. V. (2007). The Lherz spinel lherzolite: refertilised rather than pristine mantle. *Earth and Planetary Science Letters* **259**, 599–612.
- Malkovets, V. G., Griffin, W. L., O'Reilly, S. Y. & Wood, B. J. (2007). Diamond, subcalcic garnet and mantle metasomatism: Kimberlite sampling patterns define the link. *Geology* **35**, 339–342.
- Maruoka, T., Kurat, G., Dobosi, G. & Koeberl, C. (2004). Isotopic fractionation of carbon in diamonds of diamondites: Record of mass fractionation in the upper mantle. *Geochimica et Cosmochimica Acta* **68**, 1635–1644.
- McCammon, C. A., Griffin, W. L., Shee, S. H. & O'Neill, H. St. C. (2001). Oxidation during metasomatism in ultramafic xenoliths from the Wesselton kimberlite, South Africa. *Contributions to Mineralogy and Petrology* **141**, 287–296.
- McDonough, W. F. & Sun, S.-S. (1995). The composition of the Earth. *Chemical Geology* **120**, 223–253.
- Mearns, E. W. (1986). Sm–Nd ages for Norwegian garnet peridotites. *Lithos* **19**, 269–278.
- O'Neill, C. J., Moresi, L. & Jaques, A. L. (2005). Geodynamic controls on diamond deposits: Implications for Australian occurrences. *Tectonophysics* **404**, 217–236.
- O'Reilly, S. Y. & Griffin, W. L. (2006). Imaging chemical and thermal heterogeneity in the sub-continental lithospheric mantle with garnets and xenoliths: Geophysical implications. *Tectonophysics* **416**, 289–309.
- O'Reilly, S. Y., Griffin, W. L., Poudjom Djomani, Y. & Morgan, P. (2001). Are lithospheres forever? Tracking changes in subcontinental lithospheric mantle through time. *GSA Today* **11**, 4–9.
- Pearson, N. J., Griffin, W. L., Doyle, B. J., O'Reilly, S. Y., van Acherbergh, E. & Kivi, K. (1999). Xenoliths from kimberlite pipes of the Lac de Gras area, Slave Craton, Canada. In: Gurney, J. J., Gurney, J. L., Pascoe, M. D. & Richardson, S. H. (eds) *Proceedings of the 7th International Kimberlite Conference*. Cape Town: Red Roof Design, pp. 644–658.
- Piccardo, G. B., Müntener, O., Zanetti, A., Romairone, A., Bruzzone, S., Poggi, E. & Spagnolo, G. (2004). The Lanzo South peridotite: melt/peridotite interaction in the mantle lithosphere of the Jurassic Ligurian Tethys. *Ophioliti* **29**(1), 37–62.
- Poudjom Djomani, Y. H., O'Reilly, S. Y., Griffin, W. L. & Morgan, P. (2001). The density structure of subcontinental lithosphere: Constraints on delamination models. *Earth and Planetary Science Letters* **184**, 605–621.
- Rampone, E., Piccardo, G. B., Vannucci, R., Bottazzi, P. & Zanetti, A. (1994). Melt impregnation in ophiolitic peridotite: an ion microprobe study of clinopyroxene and plagioclase. *Mineralogical Magazine* **58A**, 756–757.
- Rudnick, R. L., McDonough, W. F. & Chappell, B. W. (1993). Carbonatite metasomatism in the northern Tanzanian mantle: petrographic and geochemical characteristics. *Earth and Planetary Science Letters* **114**, 463–475.

- Scambelluri, M., Pettko, T. & van Roermund, H. L. M. (2008). Majoritic garnets monitor deep subduction fluid flow and mantle dynamics. *Geology* **36**, 59–62.
- Simon, N. S. C., Irvine, G. J., Davies, G. R., Pearson, D. G. & Carlson, R. W. (2003). The origin of garnet and clinopyroxene in 'depleted' Kaapvaal peridotites. *Lithos* **71**, 289–322.
- Simon, N. S. C., Carlson, R. W., Pearson, D. G. & Davies, G. R. (2007). The origin and evolution of the Kaapvaal cratonic lithospheric mantle. *Journal of Petrology* **48**, 589–565.
- Smith, D. & Boyd, F. R. (1987). Compositional heterogeneities in a high-temperature lherzolite nodule and implications for mantle processes. In: Nixon, P. H. (ed.) *Mantle Xenoliths*. New York: John Wiley, pp. 551–562.
- Smith, D., Griffin, W. L. & Ryan, C. G. (1993). Compositional evolution of high-temperature sheared lherzolite PHN1611. *Geochimica et Cosmochimica Acta* **57**, 605–613.
- Song, S., Zhang, L. & Niu, Y. (2004). Ultra-deep origin of garnet peridotite from the North Qaidam ultrahigh-pressure belt, northern Tibetan Plateau, NW China. *American Mineralogist* **89**, 1330–1336.
- Spengler, D., Von Roermund, H. M. L., Drury, M., Ottolini, L., Mason, P. R. D. & Davies, G. R. (2006). Deep origin and hot melting of an Archean orogenic peridotite massif in Norway. *Nature* **440**, 913–209.
- Stachel, T., Viljoen, F., Brey, G. P. & Harris, J. W. (1998). Metasomatic processes in lherzolitic and harzburgitic domains of diamondiferous lithospheric mantle: REE in garnets from xenoliths and inclusions in diamonds. *Earth and Planetary Science Letters* **159**, 1–12.
- Stixrude, L. & Lithgow-Bertelloni, C. (2005). Mineralogy and elasticity of the oceanic upper mantle: Origin of the low-velocity zone. *Journal of Geophysical Research* **110**, doi:10.1029/2004JB002965.
- Van der Wal, D. & Bodinier, J.-L. (1996). Origin of the recrystallisation front in the Ronda peridotite by km-scale pervasive porous melt flow. *Contributions to Mineralogy and Petrology* **122**, 387–405.
- Van Roermund, H. L. M., Drury, M. R., Barnhoorn, A. & De Ronde, A. (2000). Super-silicic garnet microstructures from an orogenic garnet peridotite, evidence for an ultra-deep (>6 GPa) origin. *Journal of Metamorphic Geology* **18**, 135–147.
- Van Roermund, H. L. M., Drury, M. R., Barnhoorn, A. & De Ronde, A. (2001). Relict majoritic garnet microstructures from ultra-deep orogenic peridotites in western Norway. *Journal of Petrology* **42**, 117–130.
- Walter, M. J. (1998). Melting of garnet peridotite and the origin of komatiite and depleted lithosphere. *Journal of Petrology* **39**, 29–60.
- Walter, M. J. (1999). Melting residues of fertile peridotite and the origin of cratonic lithosphere. In: Fei, Y., Bertka, C. M. & Mysen, B. O. (eds) *Mantle Petrology: Field Observations and High Pressure Experimentation: a Tribute to Francis F. (Joe) Boyd*. Geochemical Society, Special Publication **6**, 225–240.
- Wyatt, B. A., Mitchell, M., White, B., Shee, S. R., Griffin, W. L. & Tomlinson, N. (2002). The Brockman Creek kimberlite, east Pilbara, Australia. *Extended Abstracts of 4th International Archean Symposium. AGSO-Geoscience Australia Record* **2001/37**, 208–211.
- Xu, X., O'Reilly, S. Y., Griffin, W. L. & Zhou, X. (2000). Genesis of young lithospheric mantle in southeastern China: a LAM-ICPMS trace element study. *Journal of Petrology* **41**, 111–148.
- Xu, X., Griffin, W. L., O'Reilly, S. Y., Pearson, N. J., Geng, H. & Zheng, J. P. (2008). Re–Os isotopes in mantle xenoliths from eastern China: age constraints and evolution of lithospheric mantle. *Lithos* **102**, 43–64.
- Ye, K., Cong, B. & Ye, D. (2000). The possible subduction of continental material to depths greater than 200 km. *Nature* **407**, 734–736.
- Zheng, J., Griffin, W. L., O'Reilly, S. Y., Lu, F., Wang, C., Zhang, M., Wang, F. & Li, H. (2004). 3.6 Ga lower crust in central China: new evidence on the assembly of the North China Craton. *Geology* **32**, 229–232.
- Zheng, J. P., Griffin, W. L., O'Reilly, S. Y., Zhang, M., Pearson, N. J. & Luo, Z. (2006a). The lithospheric mantle beneath the southern Tianshan area, NW China. *Contributions to Mineralogy and Petrology* **151**, 457–479.
- Zheng, J. P., Griffin, W. L., O'Reilly, S. Y., Zhang, M., Pan, Y., Pearson, N. J. & Lin, G. (2006b). Widespread Archean basement beneath the Yangtze Craton. *Geology* **34**, 417–420.
- Zheng, J. P., Griffin, W. L., O'Reilly, S. Y., Yu, C., Zhang, H. F., Pearson, N. J. & Zhang, M. (2007). Mechanism, timing and consequences of lithospheric modification beneath the eastern North China Craton: a regional synthesis. *Geochimica et Cosmochimica Acta* **71**, 5203–5225.

APPENDIX

We have computed stable assemblages and all their relevant properties by a free energy minimization procedure [see details given by Connolly (2005) and Afonso *et al.* (2008)] within the system CFMAS (CaO–FeO–MgO–Al₂O₃–SiO₂). These five major oxides make up more than 98% of the Earth's mantle, and therefore they are an excellent starting basis to model mantle phase equilibria. Two thermodynamic databases were employed: one is based on the work of Holland & Powell (1998), as updated by Connolly (2005); the other is that of Stixrude & Lithgow-Bertelloni (2005). Solution models adopted for these databases are summarized in Table A1, together with their respective notation and formulae.

Properties and modal proportions shown in Table 2 were computed at temperatures and pressures corresponding to 100 and 200 km depth along a 40 mW/m² conductive geotherm. The latter follows a parameterization of the type P (kbar) = $C_0(T^2) + C_1T + C_2$, where T is temperature in centigrade, $C_0 = 1.786 \times 10^{-5}$, $C_1 = 2.742 \times 10^{-2}$, and $C_2 = -1.1988$.

Table A1: Solution models, and their notation and formulae

Solid solution (HP)	Formula	Ref.	Solid solution (STX)	Formula	Ref.
OI	$Mg_{2x}Fe_{2(1-x)}SiO_4$	1	OI	$[Mg_xFe_{1-x}]_2SiO_4$	4
Opx	$Mg_{x(2-y)}Fe_{(1-x)(2-y)}Al_2Si_{2-y}O_6$	2	Opx	$[Mg_xFe_{1-x}]_{2-y}Al_2Si_{2-y}O_6$	4
Cpx	$Na_{1-y}Ca_yMg_{xy}Fe_{(1-x)y}Al_ySi_2O_6$	2	Cpx	$Ca_{1-y}[Mg_xFe_{1-x}]_{1+y}Si_2O_6$	4
Gt	$Fe_{3x}Ca_{3y}Mg_{3(1-x-y)}Al_2Si_3O_{12}$ $x + y \leq 1$	1	Gt	$Fe_{3x}Ca_{3y}Mg_{3(1-x+y+z/3)}Al_{2-2z}Si_{3+z}O_{12}$ $x + y \leq 1$	4
Sp	$Mg_xFe_{1-x}Al_2O_3$	1	Sp	$Mg_xFe_{1-x}Al_2O_4$	4
Feldspar	$K_yNa_xCa_{1-x-y}Al_{2-x-y}Si_{2+x+y}O_8$ $x + y \leq 1$	3	*		

HP, Holland & Powell (1998); STX, Stixrude & Lithgow-Bertelloni (2005). 1, Holland & Powell (1998); 2, Holland & Powell (1996); 3, Fuhrman & Lindsley (1988); 4, Stixrude & Lithgow-Bertelloni (2005).

*When using the STX database, the low-pressure Al-bearing phase is assumed to be pure anorthite.